Phase-contrast microtomography of thin biomaterials

F. RUSTICHELLI*, S. ROMANZETTI†, B. DUBINI
Istituto di Scienze Fisiche, Università degli Studi di Ancona and INFM, Via P. Ranieri 65, 60131 Ancona, Italy
E-mail: isf@alisf1.univpm.it

E. GIRARDIN
Università di Ancona, Facoltà d'Ingegneria, Dipartimento di Fisica e Ingegneria dei Materiali e del Territorio, Via Brecce Bianche and INFM, 60131 Ancona, Italy

C. RAVEN, A. SNIGIREV
ESRF, 38043 Grenoble, France

G. RIZZI
Biocoating, Via Volta 3, Rubbiano di Solignano, 43040 Parma, Italy

Phase-contrast microtomography, performed at the beamline ID 22 of the European Synchrotron Radiation Facility (ESRF, Grenoble, France), is demonstrated for high-resolution 3-D imaging of a hydroxyapatite sample. The technique, which relies on phase contrast imaging, gives the possibility to observe features inside samples with negligible absorption contrast. The positive results obtained suggest a possible future investigation of the influence of the distribution of pores and defects inside biomaterial coatings, on the growth of osteoblast cells.

1. Introduction

X-ray phase-contrast imaging, a technique related to refractive index distribution in the sample, is a very useful tool for the investigation of materials in which X-ray absorption-contrast is negligible. As previous works have shown, phase-contrast imaging enhances the images compared to the ones obtained by conventional absorption-contrast and, most important, it is able to reveal internal details of either very thin objects or those composed of light elements which are almost transparent to conventional X-ray imaging techniques [1–7]. Furthermore, given the nature of the involved interaction, namely refraction, the irradiated materials experience a low deposition of energy.

Phase-contrast imaging can be realised in many different ways [1, 2, 9] but if applied concurrently with third generation synchrotron radiation sources, in which the spatial coherence and brilliance of the X-ray beams are remarkably high, the investigations can be performed using a very simple set-up and in a very short time [10, 11]. In this case, a spatially coherent and high energetic (~ 20 keV) monochromatic X-ray beam penetrates into the object under investigation undergoing low attenuation and high phase shift caused by the non-uniform distribution of refractive indexes [8]. As the X-ray beam continues to propagate through the object the so-generated phase distortions develop into intensity modulations, i.e. phase contrast images, which are recorded at sub-micron resolution by a high-resolution detector.

Refraction being the dominant interaction as the photon energy increases, it is clear that phase-contrast imaging has many advantages compared to absorption-contrast imaging. In particular, it overcomes the limitations of imaging light density materials and improves the resolution of classical imaging methods such as X-ray radiography and tomography, which depending on the applications cannot be better than 7 μm [12]. On the basis of these facts, the technique of phase-contrast microtomography has been recently developed [14, 15]. Such a technique exploits the same idea of classical computer tomography (CT) the only difference being that the images recorded during the rotation of the specimen about the tomographic axis are obtained using the phase-contrast imaging method. This means that for each sample's rotation about the tomographic axis the refractive index gradients in the sample are imaged on a sub-micrometer scale. The integrated phase-contrast images, called projections, recorded for each angle of sample's rotation, and combined together using a filtered back-projection algorithm, are converted into the 3-D spatial distribution of the refractive indexes' inhomogeneities. Eventually, the 3-D distribution of ''phase shifts per voxel'', which

*Author to whom all correspondence should be addressed.
†Present Address: MR Group – Institute of Medicine, Research Centre Juelich, D52425 Germany.

can be approximately seen as the sample's mass density distribution, can be virtually sectioned to look at internal structures of the sample without physically cutting it.

In this paper we will show the results of phase-contrast microtomography performed at the beamline ID 22 of the European Synchrotron Radiation Facility (ESRF, Grenoble, France) on a hydroxyapatite (HAp) sample.

Hydroxyapatite and related calcium phosphates have been studied for many years as implant materials due to their similarity with bone. HAp coatings, deposited by plasma spraying on a substrate, mainly Ti–6Al–4V alloys, combine the superior mechanical performance of the metal component with the excellent biological responses of HAp. HAp is totally biocompatible, it does not create inflammatory reaction or toxicity and is resistant to physiological corrosion. Moreover, HAp is a bioactive material as it allows chemical reactions at the interface between implant and osseous tissues. In addition, HAp promotes bone growth [16, 17], reduces the healing time, strengthens the implant–bone attachment, increases tolerance of surgical inaccuracies and avoids ion release from the coating substrate acting as a barrier between substrate and bone.

The aforementioned properties are not so important in the short time but may increase long-term implant stability.

Another very important property of the HAp is its interconnected porous or bone-like morphology. This feature is highly significant, as it supports the growth of bone tissue through the pores (osteoconduction). Since osteons' average diameter ranges between 180 and 250 μm, and communicate through Volksmann channels, the size of the interconnected pores should have similar dimensions. However, as an increase of the average pore size reduces the compressive strength of the structure, to have HAp with controlled pore size is an important requirement for clinical applications.

The purpose of this methodological work is to demonstrate the possibility of precise shape and dimension determination of the interconnected porous structure of HAp by phase-contrast microtomography.

TABLE I Parameters of the plasma torch used for the deposition of the studied HAp coating

Intensity (A)	Voltage (V)	Power (W)	Ar feed rate (l/min)	N_2 feed rate (l/min)	Spraying distance (mm)
350	67	23 500	20	15	75

2. Samples and experimental details

The investigated sample is an HAp coating deposited by plasma spraying on a TA6V alloy substrate. Pure crystalline HAp powder ($Ca_{10}(PO_4)_6(OH)_2$) of size distribution 5–20 μm has been used to prepare the coating. The plasma spraying has been performed using the parameters reported in Table I.

The substrate has been sandblasted before deposition to allow a better adhesion of the coating. The HAp coating was highly crystalline.

Previous scanning electron microscopy (SEM) investigations showed a distribution of the equivalent pore diameter ranging between 9 and 420 μm [13]. The sample has been mechanically removed from the alloy substrate and cut to fit the field of view of the phase-contrast apparatus to a final dimension of about $600 \times 450 \times 250\,\mu m^3$.

It must be noted that during the cutting process of the sample it was not possible to prevent the introduction of defects in the inner structure. However, defects introduced by the cut, which are the result of highly localised stresses, are very interesting features which can be used to validate the technique in view of forthcoming quantitative analysis.

Fig. 1 depicts the experimental set-up for phase-contrast microtomography at the beamline ID22 of the European Synchrotron Radiation Facility (ESRF) in Grenoble, France. The apparatus is relatively simple since it requires only a monochromatic beam, a rotating sample stage and a high-resolution X-ray detecting system [15]; the latter is composed by a transparent luminescent screen (scintillator) combined with a diffraction-limited microscope objective to magnify the X-ray image onto a charge-coupled device (CCD) camera [18]. Within the field of view of the instrument

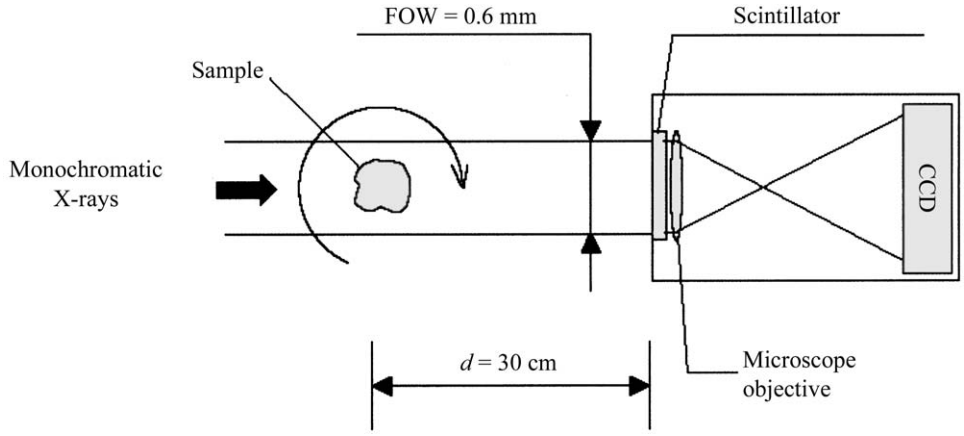

Figure 1 Scheme of the experimental set-up for the phase-contrast microtomography at the beamline ID 22 at the ESRF Grenoble, France. The monochromatic beam impinges on the sample mounted on a rotating stage. The image resulting from the interaction between the monochromatic coherent beam and the sample is converted into light by a transparent luminescent screen located at $D = 30$ cm downstream. The optical image is magnified by a microscope eyepiece onto the CCD.

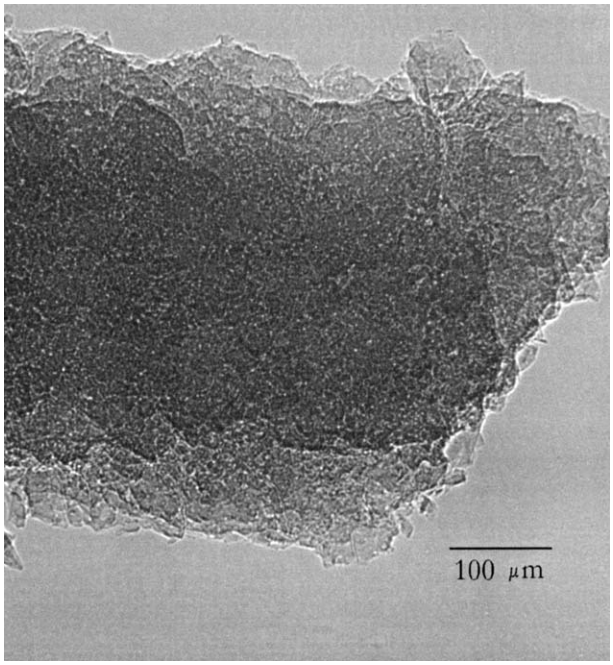

Figure 2 Phase-contrast image of a HAp sample recorded at 30 cm sample-to detector distance. The porous structure is visible and integrated over the thickness of the sample. The pixel size is 0.6 μm.

$(600 \times 600\,\mu m^2)$, the achievable spatial resolution is 0.6 μm.

The sample, mounted in the horizontal direction to exploit the higher coherence of the beam in the vertical direction [13], is fixed on top of a goniometer head. As explained in Baruchel *et al*. [7], to perform phase-contrast microtomography, it is first necessary to determine the distance between the sample and detector system to allow in-line phase-contrast images to be recorded. At the energy of 12 keV the optimum distance was found to be 30 cm and the exposure time to be 2 s. The image recorded using such parameters is reported in Fig. 2. Here, the HAp interconnected pore structure is well revealed. Once the distance was fixed, the recording of the projections from different angles sample's tomographic axis started.

In order to reconstruct the cross-sectional structure of the sample, 500 phase-contrast images like the one in Fig. 2 were recorded at equi-spaced angular rotations of the tomographic axis in the interval between 0 and 180°. Using a standard tomographic filtered backprojection algorithm [18] the projections were processed to obtain a 3-D image. The total recording time was approximately 3 h.

3. Results and discussion

The small thickness and the porosity of the sample are critical factors in this demonstration study. In fact, the thickness of the HAp coatings is very small (< 500 μm), hence little information can arise from X-ray absorption-contrast imaging techniques. Moreover the distribution of the equivalent diameters of the pores, which was previously evaluated by SEM [13], varies between 9 and 420 μm. This means that a high-resolution imaging technique is required. Fig. 3(a) shows one of the 400 reconstructed cross sections of the HAp sample. The image, reconstructed as described in the previous section, has a pixel dimension of 0.6 μm and a pixel aspect ratio of 1 : 1.

At first sight, the porous structure of the HAp is clearly evident and a large number of cracks spread in many different directions. The origin of the cracks is believed to be primarily due to the sample preparation method. These defects allow the technique to be tested. Eventually, it must be noticed that the presence of rings artefacts in the image is due to defects in the CCD camera that in any case do not prevent the extraction of information about the sample [19].

In Fig. 3(b) is shown the cross section of the sample taken 200 μm away from the one presented in Fig. 3(a). It is clear that the sample's morphology is the same in both the images. However, in Fig. 3(b) the pores are distributed in different sites in respect to Fig. 3(a). Furthermore, the distribution of the pore's diameters spread from a few microns to tens of microns, confirming that a continuous interconnected structure should exist. Cracks, present in both images, extend for no more than several tens of microns, except for a long one that extends from the top to the bottom in the central part of the sample. Also, in Fig. 3 a small area of about 80 μm

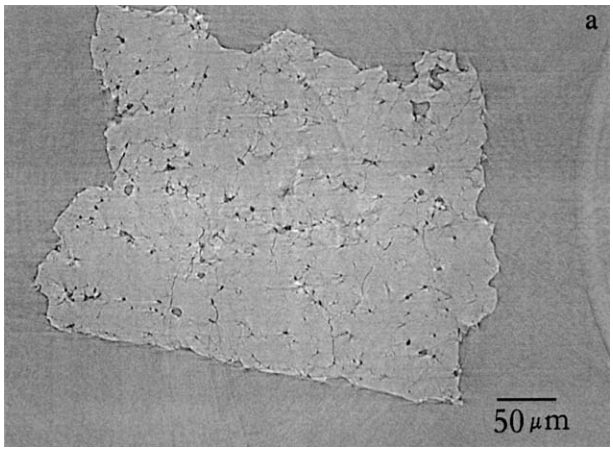

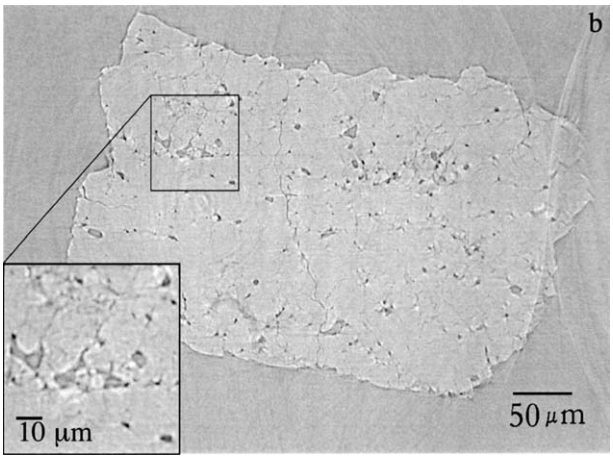

Figure 3 (a) Reconstructed cross section from 500 phase-contrast high resolution images taken over an angular range of 180°. Pixel dimension 0.6 μm and 1 : 1 aspect ratio. (b) Cross section of the sample taken 200 μm away from the cross-section reported in (a). The highlighted area shows magnified pores and cracks.

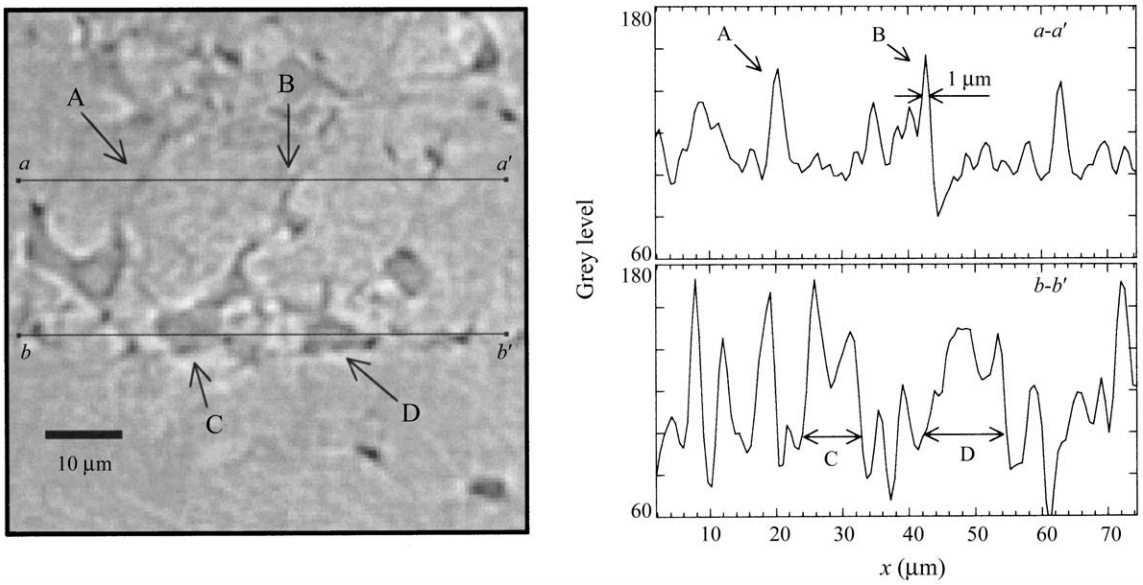

Figure 4 Quantitative evaluation of the microtomography. Along the line a–a' four peaks are noticeable, while along the line b–b' it is possible to observe the presence of pores.

has been magnified, showing some pores and cracks overlapping each other. The same magnified area (representative of the whole set of cross sections as it contains pores and cracks of different dimensions and shape) is presented again on the left-hand side of Fig. 4 in order to show the spatial achievable resolution of the phase-contrast microtomography.

In Fig. 4, two imaginary lines, a–a' and b–b' cross the area in a horizontal direction and pass through cracks and pores respectively. The right-hand side of the picture plots the variation of the grey levels of the image across the two lines. The peaks in the plots indicate that the line passes from a zone of grey to a darker one and then back to the uniform grey region. A fast variation of the plot is the indication of an edge between regions of different refraction index in the image. Furthermore, from the full width at half maximum (FWHM) of the peaks, it is possible to determine the dimensions of the pores and cracks in the direction of the lines a–a' and b–b' and to evaluate the maximal achievable resolution.

Along the line a–a', five peaks each corresponding to a crack are noticeable. Due to space limitations only the two of them labelled with the letters A and B are discussed. The first peak (A) is characterised by a peak-to-noise ratio of about 20 (in the grey levels scale) and by a FWHM of about 2 μm. The second peak (B) has a lower peak-to-noise ratio, but it is of great significance since it has a FWHW of 1 μm, which represents the maximum reachable image resolution. The line b–b' is drawn across several pores. As before, only the pores labelled C and D are discussed. From the plot of the grey values taken along this line the two pores can be evaluated in quantitative terms. In particular, the dimension in the direction of the line b–b' can be estimated measuring the distance between the tails of the plotted peaks which correspond to the pore edges. In doing so, it is possible to determine a dimension of 8 μm for the pore labelled C and of 12 μm for the pore labelled D. The error on the dimension of the pores may be half the maximum resolution, i.e. 0.5 μm.

These results clearly indicate the possibility of further

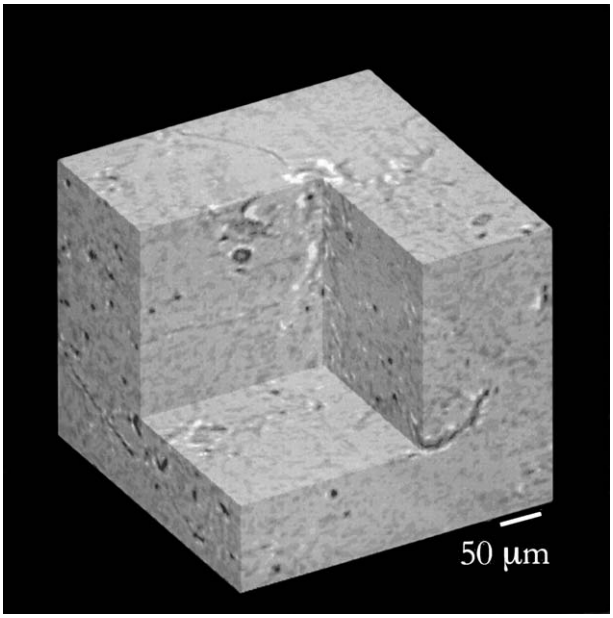

Figure 5 3-D high-resolution pictorial view of a HAp sample, obtained superimposing the full set of reconstructed cross sections.

non-destructive and quantitative analysis of HAp coatings to determine the distribution of equivalent diameters. Finally, Fig. 5 shows a 3-D reconstruction of the HAp coating generated by the superposition of the 400 reconstructed cross sections. It can be seen that also in this case a spatial resolution of few tens microns can be obtained, whereas in current medical devices for CT the spatial resolution is of the order of few hundred microns: as a consequence, the present technique presents an improvement of about two orders of magnitude, as compared to the conventional CT.

4. Conclusion

The present work showed the feasibility of investigating and imaging at 3-D level the microstructure of thin biomaterials, in particular of HAp coatings, with a spatial resolution higher by two orders of magnitude, as

compared to conventional medical tomographic devices. Phase-contrast microtomography, based on phase-contrast effect gives the possibility to observe features inside samples with negligible absorption. The positive results obtained suggest the possibility of investigating how pore size in biomaterial coatings influences the growth of osteoblast cells, and in determining which are the optimal microstructural conditions for bone growth.

5. Acknowledgments

This work was supported by INTAS 0469 entitled ''Advanced X-ray techniques for materials study based on the new generation of focusing devices'' of European Union and by the programme PURS of the National Institute for the Physics of Matter (INFM).

References

1. T. J. DAVIS, D. GAO, T. E. GUREYEV, A. W. STEVENSON and S. W. WILKINS, *Nature* **373** (1995) 595.
2. S. W. WILKINS, T. E. GUREYEV, D. GAO, A. POGANY and A. W. STEVENSON, *ibid.* **384** (1995) 335.
3. V. N. INGAL and E. A. BELIAEVSKAYA, *J. Phys. D: Appl. Phys.* **28** (1995) 2314.
4. V. N. INGAL and E. A. BELIAEVSKAYA, *Phys. Med.* **12** (1996) 75.
5. V. N. INGAL and E. A. BELIAEVSKAYA, *Tech. Phys.* **42** (1997) 59.
6. E. A. BELIAEVSKAYA, F. GAMBACCINI, V. N. INGAL, A. A. MANUSHKIN, F. RUSTICHELLI and S. SH. SHILSTEIN, *Phys. Med.* **14** (1998) 19.
7. J. BARUCHEL, A. LODINI, S. ROMANZETTI, F. RUSTICHELLI and A. SCRIVANI, *Biomaterials* **22** (2001) 1515.
8. M. BORN and E. WOLF, in ''Principles of Optics'', 6th edn (Pergamon, Oxford, 1980).
9. U. BONSE and H. HART, *Appl. Phys. Lett.* **6** (1965) 155.
10. A. SNIGIREV, I. SNIGIREVA, V. KOHN, S. KUZNETSOV and I. SCHELOKOV, *Rev. Sci. Intrum.* **66** (1995) 5486.
11. J. BARUCHEL, P. CLOETENS, M. SCHLENKER, M. PATEYRON-SALOME, J. Y. BUFFIERE, G. PEIX and F. PEYRIN, *J. Appl. Phys.* **81** (1997) 5878.
12. F. MCLAUGHLIN, J. MACKINTOSH, B. P. HAYES, A. MCLAREN, I. J. UINGS, P. SALMON, J. HUMPHREYS, E. MELDRUM and S. N. FARROW, *Bone* **30** (2002) 924.
13. E. GIRARDIN, PhD Thesis, University of Reims (1997).
14. C. RAVEN, A. SNIGIREV, I. SNIGIREVA, P. SPANNE, A. SOUVOROV and V. KOHN, *Appl. Phys. Lett.* **69** (1996) 1826.
15. P. SPANNE, C. RAVEN, I. SNIGIREVA and A. SNIGIREV, *Phy. Med. Biol.* **44** (1999) 741.
16. A. MORONI, V. L. CAJA and C. SABATO, *J. Mater. Sci.: Mater. Med.* **5** (1994) 411.
17. B. C. WANG, E. CHANG and C. Y. YANG, *Mater. Chem. Phys.* **37** (1994) 55.
18. A. KOCH, C. RAVEN, P. SPANNE and A. SNIGIREV, *J. Opt. Soc. Amer.* **15** (1998) 1940.
19. C. RAVEN, *Rev. Sci. Instrum.* **69** (1998) 2978.

Received 28 August 2002
and accepted 29 October 2003